Experimental verification of an adaptive optical multi-aperture receive antenna for laser space communications

Klaus H. Kudielka, Wolfgang M. Neubert, Arpad L. Scholtz, Walter R. Leeb

Institut für Nachrichtentechnik und Hochfrequenztechnik, Technische Universität Wien
Gußhausstraße 25/389, A-1040 Wien, Austria

ABSTRACT

The feasibility of phased telescope arrays for coherent optical space communications is demonstrated by a proof-of-concept laboratory experiment. The incident optical power is collected by four subtelescopes and coherently combined into a single monomode output fiber. The implemented optical receive array antenna is self-phasing, i.e. the optical subfield pistons are automatically adapted with respect to the direction of the incident wavefront. The telescope array is completely independent of any subsequent receiver and of the data modulation format employed. Our experimental setup operates at a wavelength of 1064nm. With an optical input power of 1nW per subaperture, the system efficiently combines the optical input subwaves and responds to a step-shaped change of the input wavefront direction within 1ms.

1. INTRODUCTION

Phased telescope arrays allow to correct atmospheric turbulence[1,2,3], to obtain high angular resolution images by long-baseline interferometry[4], to implement wide field-of-view imaging systems[5], or to coherently receive or transmit optical radiation[6,7]. We are concerned with telescope arrays for coherent optical space communications. Following microwave phased array antennas, one can use optical multi-aperture receive antennas for non-mechanical, self-adaptive fine steering of the main lobe direction. Additional benefits over single, large telescopes are modularity, implicit redundance, and reduced overall mass.

A multi-aperture receive antenna requires a mechanism which combines the optical fields collected by subtelescopes into a single optical output field. The wavefront of the optical output field should be properly shaped for efficient superposition with a local laser oscillator, as it is employed in a coherent optical receiver. We investigated various beam-combining principles and found coaxial superposition to be optimum in the sense that a subsequent optical heterodyne receiver achieves maximum electrical intermediate frequency power[8].

Coaxial subfield superposition can be achieved either in the optical regime (by beam splitters or fiber directional couplers) or in the electrical intermediate frequency domain (by RF directional couplers). The electrical approach, already demonstrated by Mercer[6], is very complex. High-data-rate receiver electronics are required for every single subtelescope path. We decided in favour of optical subfield superposition. This results in a much simpler, transparent array antenna system which operates independently of the subsequent optical receiver.

2. EXPERIMENTAL SETUP

To demonstrate the feasibility and the capabilities of phased telescope arrays operating in receive mode, we implemented a proof-of-principle laboratory experiment. Figure 1 shows the block diagram of the experimental four-aperture receive antenna. The system operates at a wavelength of 1064nm. Four closely spaced lenses couple the approximately homogeneous plane input wave into four polarization-maintaining single-mode fibers. The optical power coupled into each fiber amounts to some 1nW. Piezo-electric fiber stretchers set the relative phases (pistons) of the optical subwaves propagating to the beam combiner. The beam combiner is realized by a cascade of three 50:50 polarization-maintaining fiber directional couplers. If the correct phase relationships prevail, the incident optical radiation is coherently collected and directed to output fiber 4. In this case fibers 1, 2, and 3 carry no optical power. Hence the optical power sensors attached to these fibers indicate whether the proper piston values are set. By driving the piezo-electric fiber stretchers, the piston control unit shown in Fig. 1 automatically adapts the pistons of the subaperture fields so that the optical powers in fibers 1, 2, and 3 are minimized. Hence, within the field of view of a single subaperture, the antenna

output power available for the subsequent receiver is automatically maximized, independent of the direction of the incident wavefront.

3. REALIZATION OF SUBUNITS

3.1. Telescope array module

Figure 2 shows the telescope array module realized. Four lenses couple the incident optical radiation into single-mode fibers. The module consists of a lens block holding four lenses arranged in a square, and of four subtelescope blocks, each of which holds a fiber end. Lens block, subtelescope blocks, and mounting supports are made of stainless steel. For each subtelescope block, the lens block has two fitting pins, ensuring highly reproducible mounting of the subtelescope blocks.

The lenses are diffraction-limited singlets. They have a focal length of 15mm and a diameter of 3mm, yielding a diffraction-limited subaperture field-of-view of 410μrad. This choice results in easy-to-meet requirements when measuring the antenna characteristics. The polarization-maintaining single-mode fibers are glued into glass capillary tubes which in turn are glued into the subtelescope blocks (see Fig. 2). Each fiber end is equipped with an AR-coated faceplate. By this measure multiple reflections within the fiber-optic setup were significantly reduced.

This very compact telescope array module provides no means for subtelescope tilt adjustment. The relative tilts (fiber end displacements) were minimized during subtelescope block assembly using the optical input wave as a reference. Each fiber end was adjusted for maximum coupling efficiency. The optimum position was fixed with a UV-curing cement.

3.2. Fiber-optic and optoelectronic elements

The experimental multi-aperture receive antenna extensively uses advanced fiber technology. The fiber-optic part consists of four piston actuators and a beam combiner which is made of three directional couplers (see Fig. 1). The fiber-optic subunits are interconnected with fusion splices.

The piston actuators were realized by piezo-electric tubes which are wrapped by the polarization-maintaining single-mode fibers. The tubes have silver electrodes fired on. By applying voltage between the electrodes the fibers are stretched, thus inducing optical path length changes. The optical loss and the residual modulation of amplitude or polarization are negligible. For ±20V input voltage, the operating range of the piston actuators amounts to ±6 wavelengths, thus guaranteeing long-term operation of the piston control unit without range overflow. Piezo resonances at 37kHz and 62kHz do not substantially influence piston control loop operation.

The beam combiner, manufactured by Canadian Instrumentation and Research, is a cascade of three polarization-maintaining single-mode 50:50 fiber directional couplers. The actual splitting ratios range from 46:54 to 50:50. The four input ports (A, B, C, D) are fed by the piston actuators. The four output ports (1, 2, 3, 4) are equipped with FC connectors. Ports 1, 2, and 3 feed optical power sensors (see Fig. 1). Output port 4, also equipped with an FC connector, may be attached to an optical receiver. For system testing, port 4 also feeds an optical power sensor.

Since we use direct detection to determine the optical power minima within fibers 1, 2, and 3, the optical power sensors have to exhibit a very low noise-equivalent optical input power (NEP). Accurate piston control at an optical input power level of 1nW per subaperture typically asks for an NEP of 10pW within a control loop bandwidth of 5kHz. With an InGaAs photodiode and a low-noise operational amplifiers we achieved an NEP of some 7pW within 5kHz.

3.3. Control electronics

To find the optical power minima within fibers 1, 2, and 3, the piston control unit employs a so-called perturbation method, outlined in Figure 3. If two optical subfields of equal powers $P_A=P_B=P$ and of phases φ_A and φ_B are applied to a symmetric fiber directional coupler, the optical power sensor detects

$$P_2 = P\left(1-\cos\left(\varphi_A-\varphi_B\right)\right) . \quad (1)$$

The desired phase difference is φ_A-φ_B=0, resulting in P_1=2P and P_2=0. An additional sinusoidal disturbance of amplitude $\Delta\varphi$ and frequency f_p is applied to the phase actuator. Hence the power sensor detects oscillations at f_p and its multiples. It is sufficient to synchronously demodulate the signal at f_p into the baseband. The resulting voltage V_{PD} is proportional to

$$P\ J_1(\Delta\varphi)\sin\left(\varphi_A-\varphi_B\right) , \quad (2)$$

where J_1 denotes the first-order Bessel function. In combination with a loop filter and an integrator this signal is used to close an optical phase-locked loop (OPLL). The perturbation frequency f_p must be significantly higher than the bandwidth of the phase-locked loop, and the perturbation amplitude $\Delta\varphi$ must be very small compared to 2π. The OPLL locks at φ_A-φ_B=0 and directs the total optical input power P_A+P_B=2P to output fiber 1.

The perturbation method was successfully implemented in various adaptive optical phased arrray systems. Bridges[1] and Pearson[2] employed different dither frequencies for each subaperture to control the phases of multiple-aperture arrays for atmospheric turbulence compensation and adaptive glint tracking.

For the experimental four-aperture receive antenna we use a single perturbation signal at f_p=10kHz. By perturbing only input fibers A and D with amplitudes $\Delta\varphi_A$=0.1rad and $\Delta\varphi_D$=-0.1rad, respectively, all phase differences can be measured. Figure 4 depicts the resulting block diagram of the control unit. To decouple the three OPLLs, the integrator outputs are linearly combined according to a simple algorithm. The resulting four control signals are applied to the piston actuators shown in Fig. 1.

Two interchangeable versions of the piston control unit were implemented. An analog piston control unit consists entirely of standard analog electronic circuits. A digital piston control unit is based on the ADSP-2101 digital signal processor. Like the analog unit, it directly attaches to the three optical power sensors (1, 2, 3) and the four piston actuators (A, B, C, D) (see Fig. 1). Since both units use the same piston control algorithm (see Fig. 4), their performance is very similar.

4. MEASURED PERFORMANCE

4.1. Test setup

The basic measurement setup is depicted in Fig. 5. As an optical input source we use the collimated output beam of a polarization-maintaining single-mode fiber. A tilt mechanism sets the direction of the wavefront approaching the telescope array unit. For slow, wide-range (±500μrad) two-axis scanning of the global antenna pattern we use two scanning galvanometers. Fast, single-axis beam steering (0.1ms) in a narrow angular range (±40μrad) is accomplished by a piezo-electric tilt mirror, permitting accurate measurement of response time and instantaneous antenna pattern. The output fiber of the telescope array system under test is connected to an optical power sensor which converts the available optical power P_{out} into a proportional voltage.

4.2. Antenna pattern

The global antenna pattern, describing the angular sensitivity of the array antenna, is defined as

$$p(\vartheta_x,\vartheta_y)=\frac{P_{out}(\vartheta_x,\vartheta_y)}{P_{out}(0,0)} \quad (3)$$

where P_{out} denotes the optical output power of the array and ϑ_x and ϑ_y are the angles of incidence. The maximum of P_{out} can be observed on-axis (ϑ_x=0,ϑ_y=0), hence $p(\vartheta_x,\vartheta_y)\le 1$. Since the implemented system is self-phasing, it automatically maximizes P_{out} for each set of incidence angles, thus directing the total available optical power $P_{avail}(\vartheta_x,\vartheta_y)$ to the antenna

output. $P_{avail}(\vartheta_x,\vartheta_y)$ is proportional to the available subaperture power $P_{sub}(\vartheta_x,\vartheta_y)$. Hence the global antenna pattern $p(\vartheta_x,\vartheta_y)$ is determined by the angular sensitivity of a single subaperture.

The global antenna pattern was measured by applying voltage to the galvanometer scanners and monitoring the optical antenna output power P_{out}. Figure 6 shows the vertical section of both the measured and the calculated global antenna pattern. Excellent correspondence has been achieved. The antenna scanning range, i.e. the full-width half-maximum range of the global antenna pattern, amounts to 410μrad.

The instantaneous antenna pattern of the self-phasing array antenna describes the instantaneous angular receiving domain. If the pistons are set so that the antenna's main lobe direction is given by $(\vartheta_{x0},\vartheta_{y0})$, but the input wave direction is different (i.e. ϑ_x,ϑ_y), the antenna output power will be decreased, since destructive interference occurs in the beam combiner. We define the instantaneous antenna pattern p_I by

$$p_I^{(\vartheta_{x0},\vartheta_{y0})}(\vartheta_x,\vartheta_y)=\frac{P_{out,I}^{(\vartheta_{x0},\vartheta_{y0})}(\vartheta_x,\vartheta_y)}{P_{out}(0,0)} \tag{4}$$

where $P_{out,I}$ denotes the instantaneous output power to be obtained, e.g., immediately after a step-shaped change of the input wave direction from $(\vartheta_{x0},\vartheta_{y0})$ to $(\vartheta_x,\vartheta_y)$.

We measured the vertical section of the instantaneous antenna pattern by steering the incident wave with a piezo-electric tilt mirror and observing the instantaneous antenna output power immediately after the change of the input wave direction. To ease the determination of $P_{out,I}$ we reduced the agility of the piston control loops by a factor of 10. Figure 6 shows excellent correspondence between the calculated and the measured instantaneous antenna pattern. The instantaneous field-of-view, i.e. the full-width half-maximum angle of the instantaneous antenna pattern, was determined to be 125μrad.

4.3. Response time

The agility of the self-phasing array antenna can be demonstrated by the response to a step-shaped change of the input wave direction (step heighth: $\Delta\vartheta$). The antenna output power $P_{out}(t)$ first decreases rapidly, as the subantenna pistons are misaligned. Then the piston control loops set the new pistons, thus increasing P_{out}. We define the response time $\tau(\Delta\vartheta)$ as the time after which P_{out} has reached 95% of its maximum. One could also define the response time as the settling time of the piston values. However, the antenna output power is the more important quantity from the receiver's viewpoint.

In order to measure the response time, τ, the optical input wave has to be steered within $\tau_s<<\tau$. This is accomplished by a piezo-electric tilt mirror. To reduce mechanical resonances, the tilt mirror is driven by the step response of a second-order Butterworth lowpass. A rise time of some τ_s=110μs could be achieved.

The steering response was measured for an input wave direction step from ϑ_y=-27μrad to ϑ_y=+27μrad. The resulting antenna output power as a function of time, $P_{out}(t)$, is depicted in Fig. 7. Depending on the exact relationship between the time of the step-shaped command and the phase of the sinusoidal perturbation signal, different traces occur. This results in a "jitter" of the antenna response if the periodic test signal is not synchronized with the perturbation signal. The measured maximum steering response time τ(54μrad) amounts to 0.78ms. Further increasing the step height $\Delta\vartheta$ also increases the response time. For a step height of 20% of the diffraction-limited divergence of a single subaperture ($\Delta\vartheta$=82μrad), e.g., the response time remains below 1ms.

4.4. Pointing accuracy

Due to the small optical input power levels involved, photo detector noise causes a stochastic phase error within each of the three piston control loops, resulting in a slight mispointing of the antenna array. The effective value of the approximately Gaussian-distributed residual phase error amounts to 54mrad for piston control loops 1 and 2, and 27mrad for piston control loop 3 (see Figs. 1 and 4). In addition, the sinusoidal perturbation signal causes a deterministic phase

error. For the present setup this second effect results in an effective piston error of 71mrad for each control loop. Figure 8 visualizes both influences and two means of quantifying their consequence.

First, the mean antenna output power is reduced. This effect is described by the phasing efficiency (PEF). If phase control were ideal, the antenna output power would not be reduced, and PEF would be 100%. Our experimental receive array antenna showed an excellent PEF of 99.7%. (The reduction due to the periodic perturbation signals is included in this value).

The second important impact is the peak reduction of antenna output power. With a certain probability Pr the output power reduction R (in percent) exceeds a certain value. From the residual phase errors, which could be determined very accurately, we calculated $Pr[R>1.03\%]=10^{-6}$. This means that with a probability of 10^{-6} the antenna output power is reduced by more than just 1.03%. (The periodic perturbation of the antenna output power causing an additional reduction of maximal 0.5% was not considered in this calculation).

5. CONCLUSION

We validated the feasibility of optical phased arrays operating in receive mode. A laboratory demonstrator was realized, showing excellent performance even at low optical input power levels. The underlying piston control concept for transparent optical self-phasing arrays can easily be expanded to more than four subapertures. It distinguishes itself by low complexity and allows very light and compact setups. Integrated optics technology can eventually be used profitably for implementing piston actuators, beam combiner, and optical power sensors. Overall, the results encourage the use of optical array antennas in coherent optical space communication links.

6. ACKNOWLEDGMENTS

The contents of this paper evolved from a research project supported by the European Space Agency (ESA). We wish to thank Alex Popescu for monitoring and promoting this work. We also thank R. Bou-Vinals, A. Friedreich, C. Köpf, H. Müller, and G. Schuster for their contributions to the realization and the testing of the experimental setup.

7. REFERENCES

1. W. B. Bridges et al., "Coherent optical adaptive techniques", Appl. Opt., Vol. 13, No. 2, pp. 291-300, Feb. 1974

2. J. E. Pearson, "Atmospheric turbulence compensation using coherent optical adaptive techniques", Appl. Opt., Vol. 15, No. 3, pp.622-631, March 1976

3. C. L. Hayes et al., "Experimental test of an infrared phase conjugation adaptive array", J. Opt. Soc. Am., Vol. 67, No. 3, March 1977

4. S. Shaklan, "Fiber optic beam combiner for multiple-telescope interferometry", Opt. Eng., Vol. 29, No. 6, pp. 684-689, June 1990

5. C. R. DeHainaut et al., "Wide field of view phased array telescope", Proc. SPIE, Vol. 1236, pp. 456-462, 1990

6. L. B. Mercer, "Adaptive coherent optical receiver array", Electron. Lett., Vol. 26, No. 18, Aug. 1990

7. W. M. Neubert et al., "Experimental implementation of an optical multi-aperture antenna for space communications", Proc. SPIE, Vol. 1522, pp. 93-102, 1991

8. W. M. Neubert et al., "Coherent optical self-phasing array antenna for space communication receivers", Proc. ECOC'93, Vol. 2, pp. 501-504, Sept. 1993

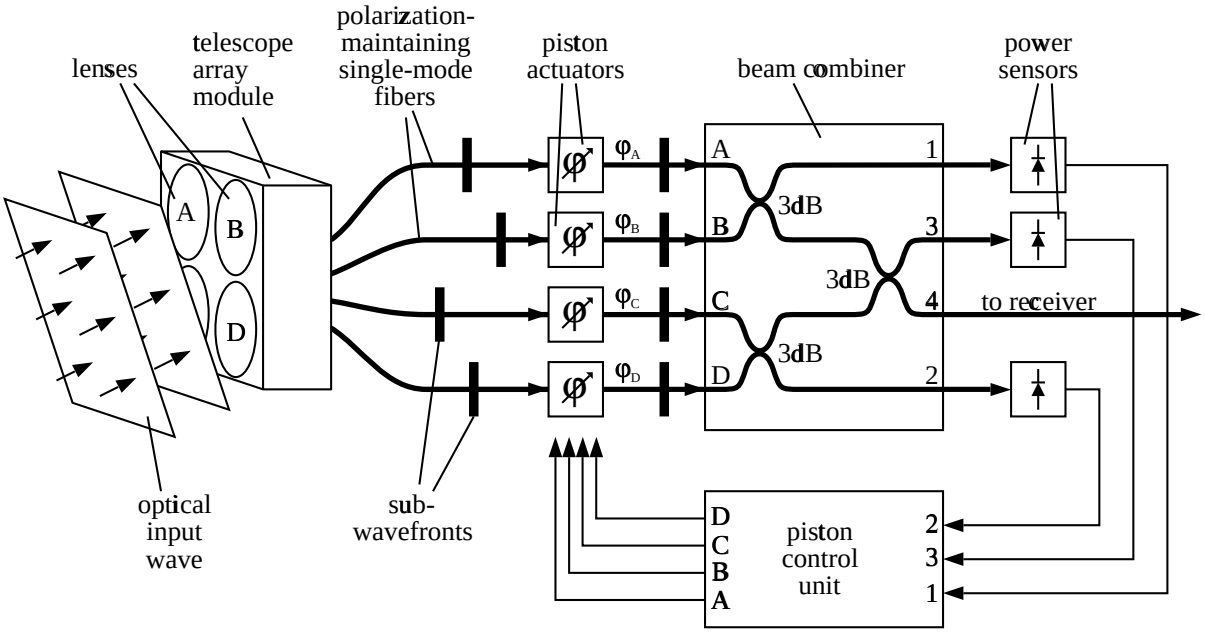

Fig. 1: Block diagram of the experimental four-aperture receive antenna

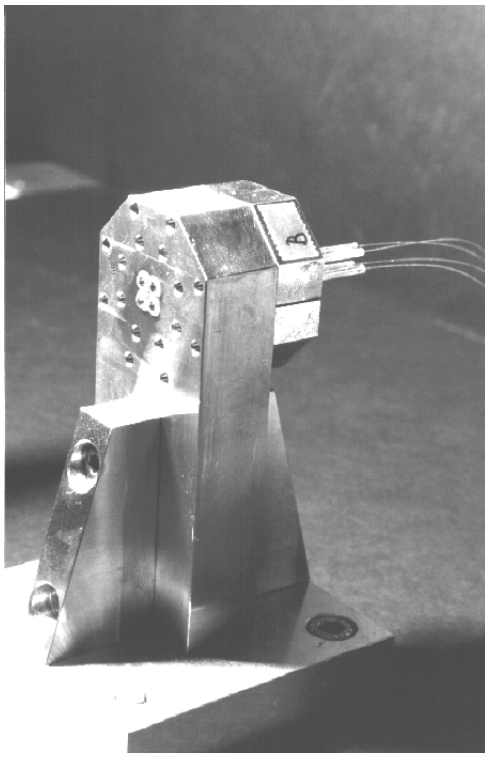

a)

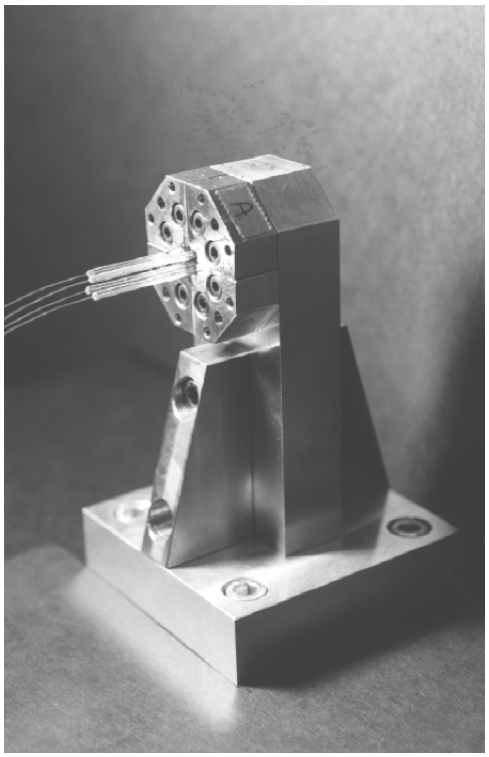

b)

Fig. 2: Telescope array module
a) front view, showing the four input lenses in the center
b) rear view, showing the telescope array's output fibers

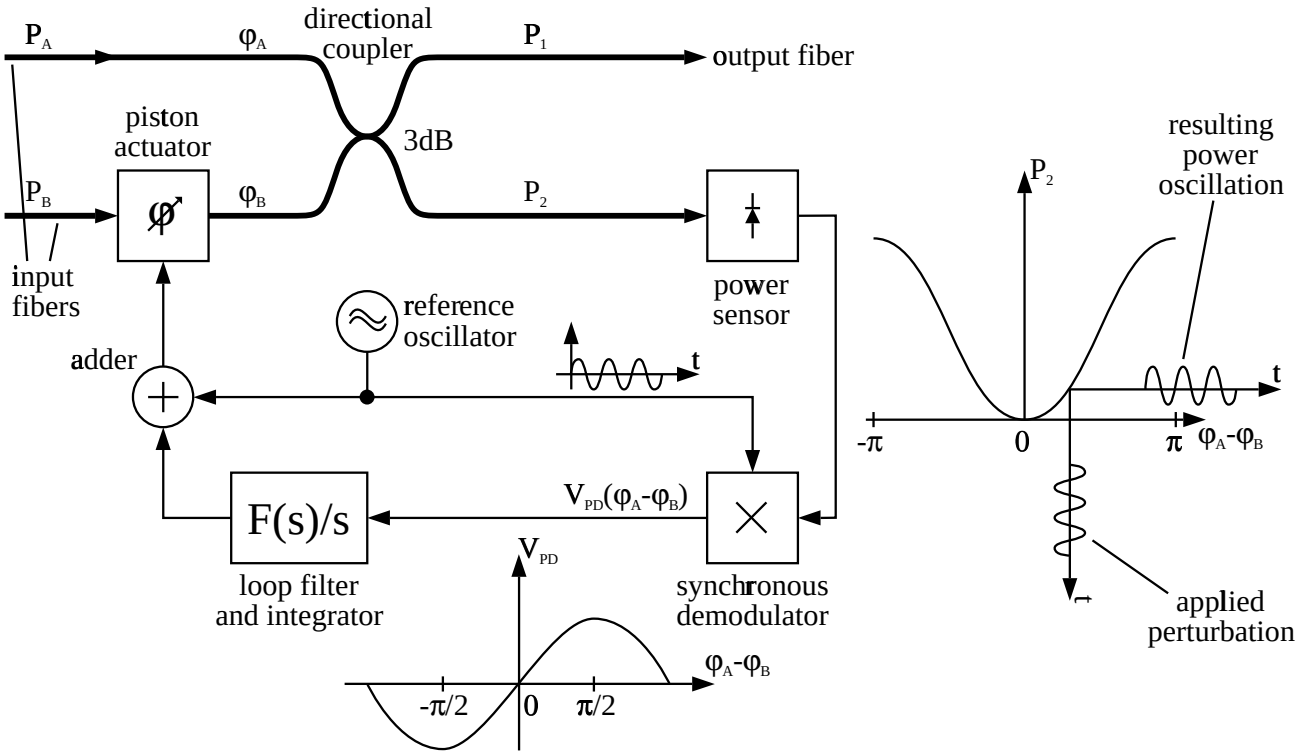

Fig. 3: An optical phase-locked loop employing a sinusoidal perturbation for piston sensing

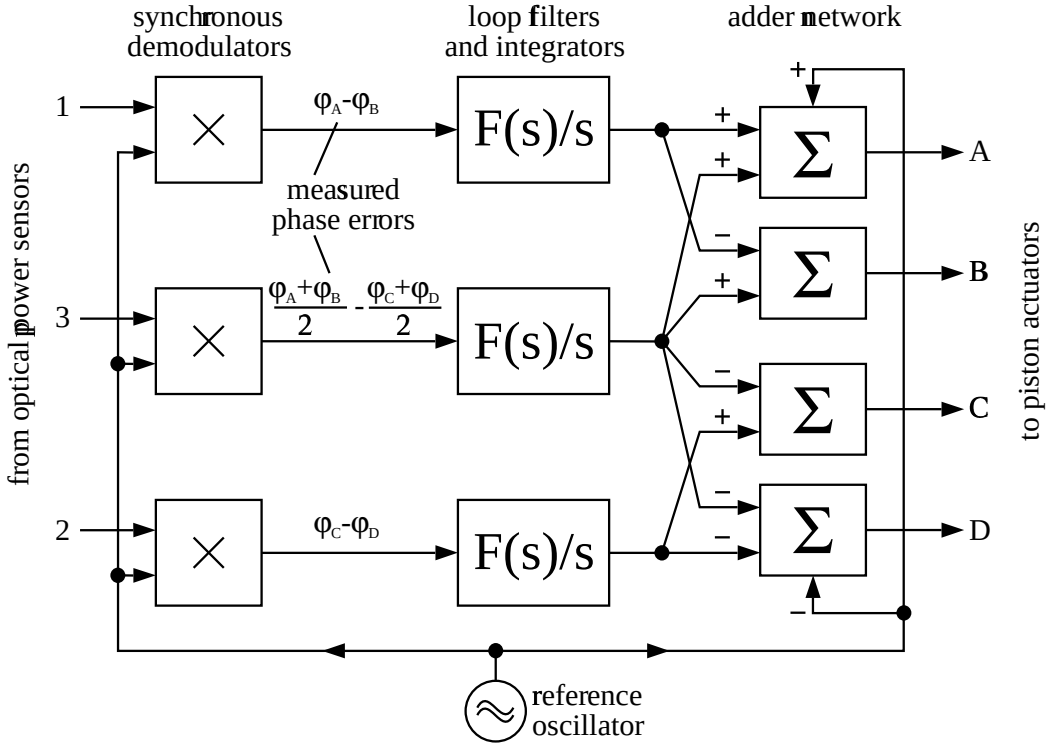

Fig. 4: Block diagram of the piston control unit

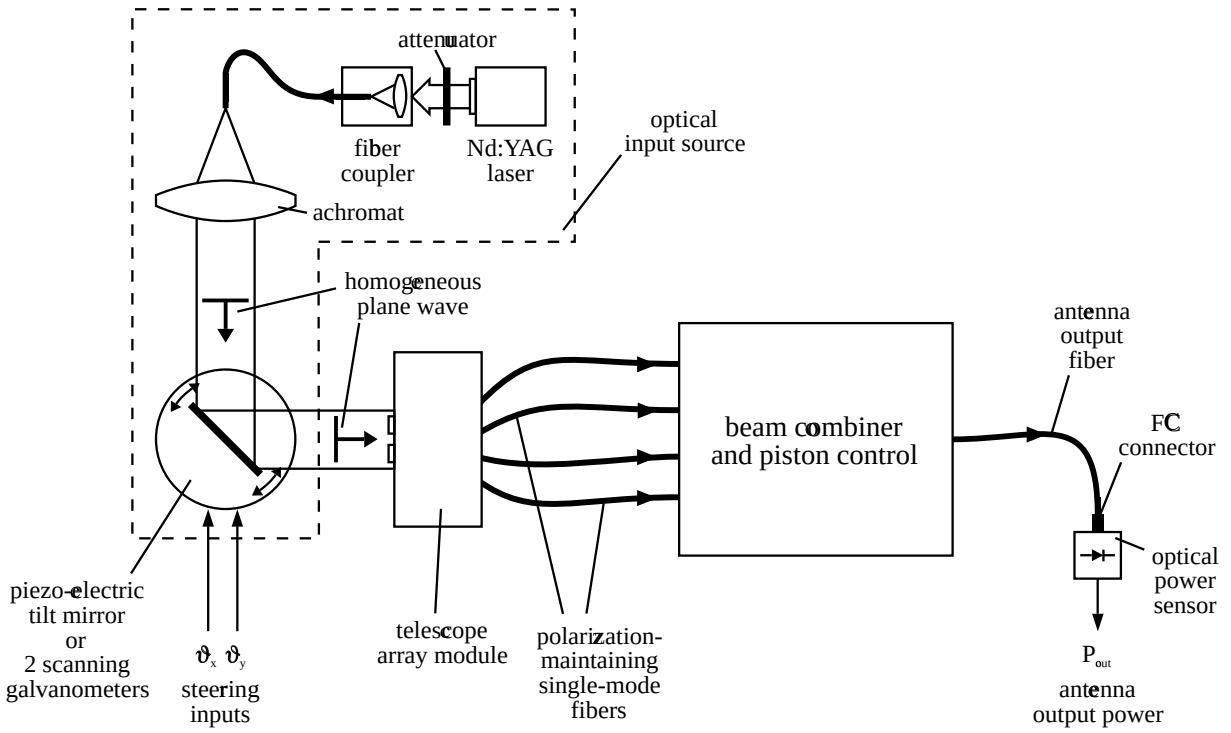

Fig. 5: Basic test setup

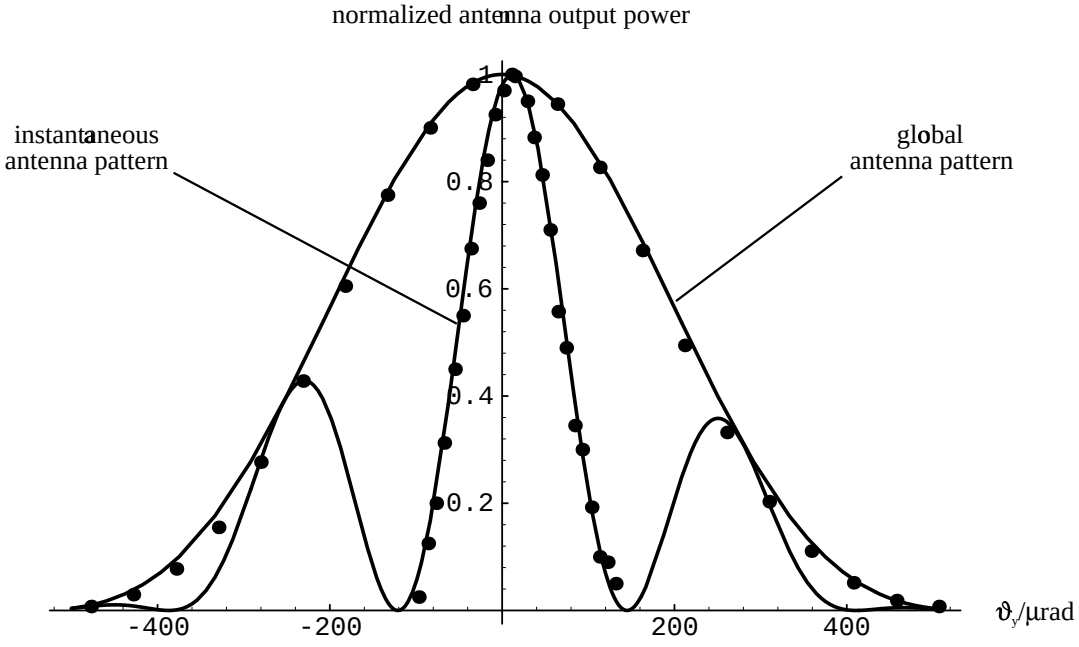

Fig. 6: Global antenna pattern and instantaneous antenna pattern (dots ... measured, solid lines ... calculated)

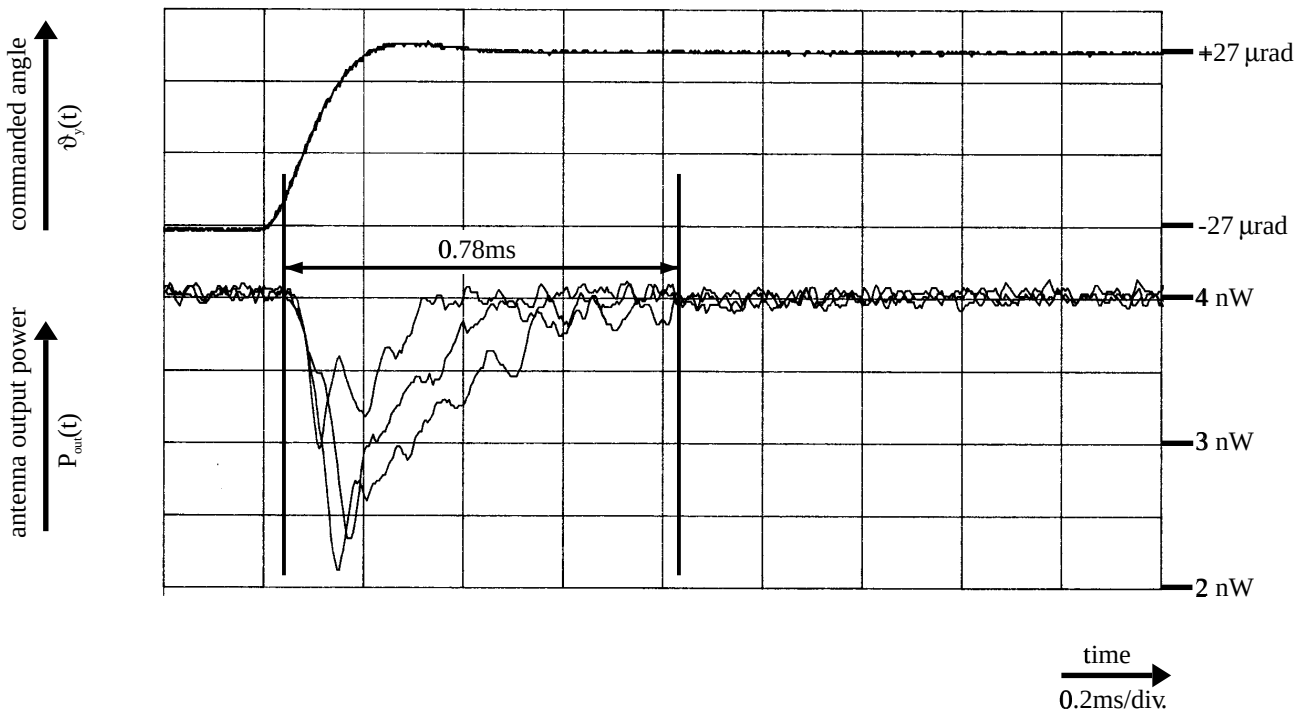

Fig. 7: Measured response to a step-shaped change of the input wave direction. The occurrence of different traces is referred to in the text. The response time amounts to 0.78ms.

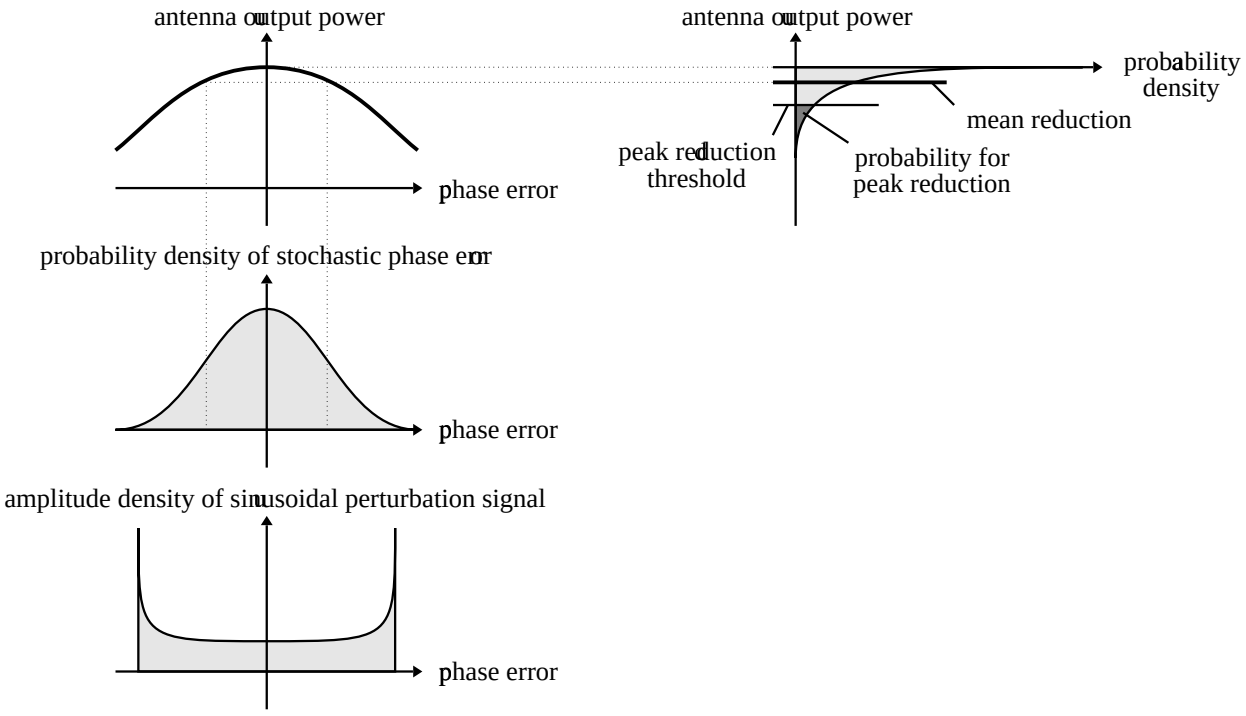

Fig. 8: Influence of the residual phase error on the distribution of the antenna output power